Urban recharge beneath low impact development and effects of climate variability and change

Michelle E. Newcomer,[1,2] Jason J. Gurdak,[1] Leonard S. Sklar,[1] and Leora Nanus[1]

Received 16 June 2013; revised 21 December 2013; accepted 26 December 2013.

[1] Understanding low impact development (LID) planning and best management practices (BMPs) effects on recharge is important because of the increasing use of LID BMPs to reduce storm water runoff and improve surface-water quality. LID BMPs are microscale, decentralized management techniques such as vegetated systems, pervious pavement, and infiltration trenches to capture, reduce, filter, and slow storm water runoff. Some BMPs may enhance recharge, which has often been considered a secondary management benefit. Here we report results of a field and HYDRUS-2D modeling study in San Francisco, California, USA to quantify urban recharge rates, volumes, and efficiency beneath a LID BMP infiltration trench and irrigated lawn considering historical El Niño/Southern Oscillation (ENSO) variability and future climate change using simulated precipitation from the Geophysical Fluid Dynamic Laboratory (GFDL) A1F1 climate scenario. We find that in situ and modeling methods are complementary, particularly for simulating historical and future recharge scenarios, and the in situ data are critical for accurately estimating recharge under current conditions. Observed (2011–2012) and future (2099–2100) recharge rates beneath the infiltration trench (1750–3710 mm yr^{-1}) were an order of magnitude greater than beneath the irrigated lawn (130–730 mm yr^{-1}). Beneath the infiltration trench, recharge rates ranged from 1390 to 5840 mm yr^{-1} and averaged 3410 mm yr^{-1} for El Niño years (1954–2012) and from 1540 to 3330 mm yr^{-1} and averaged 2430 mm yr^{-1} for La Niña years. We demonstrate a clear benefit for recharge and local groundwater resources using LID BMPs.

Citation: Newcomer, M. E., J. J. Gurdak, L. S. Sklar, and L. Nanus (2014), Urban recharge beneath low impact development and effects of climate variability and change, *Water Resour. Res.*, *50*, doi:10.1002/2013WR014282.

1. Introduction

[2] Freshwater resources in many urban environments are highly vulnerable to human pressures and climate variability and change [*Treidel et al*., 2012]. Impervious surfaces such as buildings, roads, parking lots, and compacted soil prevent infiltration of urban storm water flows and cause localized flooding, and increase contaminants in surface runoff that often overwhelm sewer systems and combined storm water-sewer flows that are often untreated [*United States Environmental Protection Agency* (*US EPA*), 2000; *Cantone and Schmidt*, 2011]. To address these concerns, urban storm water managers are increasingly using low impact development (LID) site planning to maintain or replicate the predevelopment hydrologic regime by using best management practices (BMPs) that decrease the impacts on storm water drainage systems and help maintain surface water quality [*Ando and Freitas*, 2011]. Within the overarching LID framework, BMPs are microscale and decentralized management techniques that include natural vegetated systems such as bioretention facilities, vegetated swales, pervious pavement, and infiltration basins and trenches to capture, reduce, filter, and slow storm water runoff [*US EPA*, 2000]. LID BMPs decrease peak runoff by as much as 40–90% [*Davis*, 2008; *Schlea*, 2011] and can remove and attenuate contaminants in polluted storm water by passive volatilization, photodecomposition, adsorption, microbial biotransformation, and dilution, which require minimal energy and resources [*Laws et al*., 2011]. LID is generally less expensive than traditional and centralized storm water infrastructure in the case of new development; however, the cost benefit of LID is less for retrofits of existing development [*Ando and Freitas*, 2011]. LID is also generally less expensive than constructing, operating, and maintaining facilities for wastewater treatment followed by recharging the recycled water [*Stephens et al*., 2012]. For these reasons, the U.S. Environmental Protection Agency (USEPA) is considering new regulations that would mandate LID for storm water management and evaluating the potential benefit that increasing infiltration beneath LID may have on groundwater resources [*United*

Additional supporting information may be found in the online version of this article.

[1]Department of Earth and Climate Sciences, San Francisco State University, San Francisco, California, USA.

[2]Department of Civil and Environmental Engineering, University of California, Berkeley, California, USA.

Corresponding author: J. J. Gurdak, Department of Earth and Climate Sciences, San Francisco State University, 1600 Holloway Ave., San Francisco, CA 94132, USA. (jgurdak@sfsu.edu)

0043-1397/14/10.1002/2013WR014282

States Environmental Protection Agency (*US EPA*), 2009]. In fact, implementing LID in some locations may be more driven by the potential benefit of groundwater recharge than compliance with surface-water quality regulations, particularly in areas that have substantial storm water runoff but a groundwater deficit [*Stephens et al*., 2012].

[3] While the effectiveness of LID BMPs increasing infiltration and reducing storm water runoff has been well studied and documented [*Dietz*, 2005, 2007; *Davis*, 2008; *Schlea*, 2011; *Guo et al*., 2012], the effectiveness of those BMPs enhancing urban recharge is poorly understood. The performance of LID BMPs that enhance infiltration and recharge needs to be validated [*Stephens et al*., 2012], in part, because few field-based studies have directly measured recharge beneath a BMP [*Davis et al*., 2009; *Roy-Poirier et al*., 2010]. Recharge beneath LID BMPs has been previously modeled or estimated as a percentage of precipitation or runoff. Studies estimate that between 40 and 99% of precipitation falling on the drainage area becomes recharge beneath BMPs [*Dietz*, 2005; *Dietz and Clausen*, 2006; *Ermilio and Traver*, 2006; *Endreny and Collins*, 2009; *Stephens et al*., 2012]. In Arizona, recharge beneath BMPs has been estimated as a fraction of captured runoff that does not evaporate using a curve number method [*Milczarek et al*., 2005]. *Milczarek et al*. [2007] used surface-water based regression models to estimate infiltration and then applied coefficients to estimate recharge as a percentage of infiltration. Beneath several unlined and large-scale (2000–23,500 m^2) retention ponds in a new industrial development in New Mexico, *Miller* [2006] estimated recharge as residual values from groundwater and unsaturated flow models calibrated to match observed water levels. The unlined retention ponds were estimated to enhance recharge from $<1\%$ to about 60% of on site precipitation and created a 3.0–10 m thick groundwater mound [*Miller*, 2006]. Some municipalities have implemented groundwater recharge studies for large scale and centralized managed aquifer recharge (MAR) sites, often using yearly water budgets and field-calibrated groundwater flow models to predict recharge [*Watershed Council: Los Angeles and San Gabriel Rivers*, 2000; *Hanson et al*., 2010; *Racz et al*., 2011]; however, these studies do not address or quantify small scale or spatially distributed recharge beneath LID BMPs. Findings from these prior studies indicate that recharge beneath LID BMPs is likely controlled in part by the precipitation intensity and duration, runoff characteristics of the impervious cover connected to the BMP, soil properties, including hydraulic conductivity, and the storage capacity of the BMP facility [*Shuster et al*., 2007; *Maimone et al*., 2011].

[4] Recharge is among the most difficult components of a water budget to reliably quantify because of its spatial and temporal variability [*Scanlon et al*., 2002; *McMahon et al*., 2011]. Estimating recharge beneath LID is further complicated because recharge rates and mechanisms, recharge enhancements compared to predevelopment conditions, and the characteristics of subsurface flow processes are not well characterized in urban environments [*Lerner*, 1990, 2002]. Sources of urban recharge include natural precipitation beneath permeable surfaces such as grass; irrigation on lawns, parks, and golf courses; leaking mains, sewers, and septic systems; and water drainage systems [*Lerner*, 1990, 2002]. Although substantial work has addressed the water quality of storm water infiltrating BMPs [*Schroeder*, 1995; *Dietz and Clausen*, 2005, 2006, 2008], the characteristics and quantities of subsurface flow beneath LID BMPs are not well documented [*Dietz*, 2005; *Dietz and Clausen*, 2008; *US EPA*, 2000], particularly as compared to other sources of urban recharge. Studies are needed to evaluate the effectiveness of LID BMPs to enhance recharge rates compared to other sources of urban recharge, such as irrigated lawns.

[5] The use of LID BMPs to capture storm water and enhance recharge has been suggested as an adaptive management strategy for future climate variability and change [*Stephens et al*., 2012], but this issue has not yet been studied. It is well established that interannual to multidecadal climate variability, such as from the El Niño/Southern Oscillation (ENSO), substantially affects the frequency and intensity of precipitation, drought, runoff, and streamflow [*Cayan et al*., 1992; *Dettinger and Cayan*, 1994; *Dettinger et al*., 2001; *Enfield et al*., 2001; *Labat*, 2008; *McCabe et al*., 2004; *Vicente-Serrano et al*., 2011]. ENSO is a 2–7 year quasiperiodic and coupled oceanic-atmospheric phenomenon that results from large-scale interactions between the tropical and subtropical portions of the Pacific and the Indian Ocean basins. ENSO produces variations in pressure, temperature, and precipitation patterns throughout the U.S. and other parts of the world [*Wolter and Timlin*, 1993, 1998]. During the positive ENSO (El Niño) phase, much of California and other parts of the U.S. have increased precipitation, particularly in the winter months of December–February [*Ropelewski and Halpert*, 1986]. In California, extreme precipitation events defined as a 50 year return interval of approximately 150 mm per day are strongly correlated with the El Niño phase, and conversely, the risk of precipitation extremes is reduced during the negative ENSO (La Niña) phase [*Shang et al*., 2011]. Between 1950 and 2009, urban areas in California have experienced a 6.5% per decade increase in the daily precipitation maximums; a trend that may have profound implications for future storm water infrastructure [*Mishra and Lettenmaier*, 2011]. Such findings are consistent with results from global circulation models (GCMs) that project increasing maximum daily precipitation for California by the 2060s [*Pierce et al*., 2012]. Considering that the frequency of central pacific and eastern pacific ENSO events have increased in recent decades and may be attributed to natural variability [*Yeh et al*., 2011], the expectation that ENSO statistics and the effects on local hydrology will change under anthropogenic climate change remains uncertain because of the large spread of model projections for the 21st century [*Guilyardi et al*., 2009].

[6] The effects of climate variability and change on recharge and groundwater resources have been increasingly studied in recent years [*United Nations Educational, Scientific and Cultural Organization*, 2008; *Earman and Dettinger*, 2011; *Green et al*., 2007, 2011; *Treidel et al*., 2012; *Taylor et al*., 2012]. Recharge rates and mechanisms and corresponding groundwater levels beneath natural and agricultural lands respond to ENSO and other oceanic-atmospheric phenomenon on interannual to multidecadal time scales [*Hanson et al*., 2004; *Pool*, 2005; *Fleming and Quilty*, 2007; *Gurdak et al*., 2007, 2009; *Holman et al*., 2009, 2011; *Tremblay et al*., 2011; *Perez-Valdivia et al*., 2012]. The natural variability of ENSO and the projected

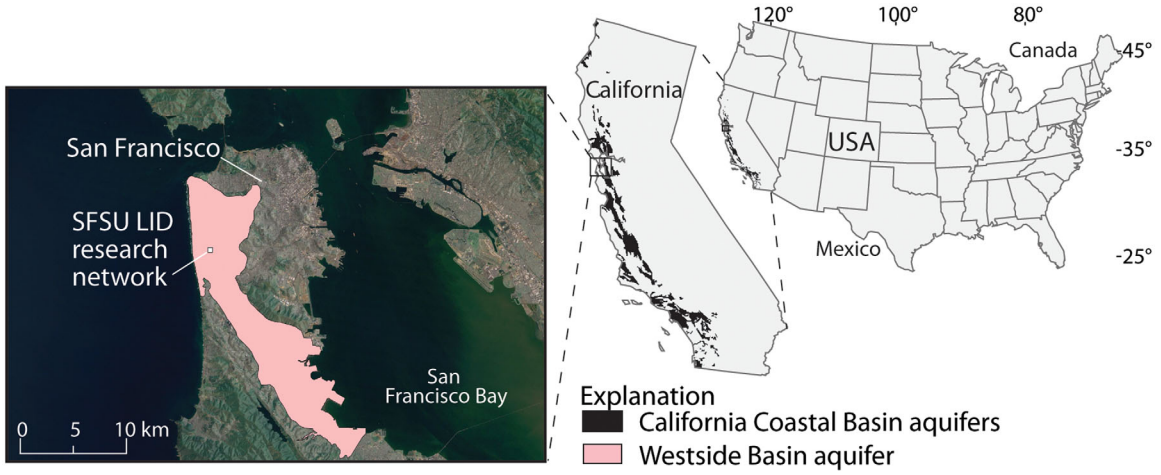

Figure 1. Map showing the location of the San Francisco State University (SFSU) low impact development (LID) research network and the Westside Basin aquifer, which is part of the California Coastal Basin aquifers. The aquifer location data are modified from the California Department of Water Resources and the U.S. Geological Survey.

increases in precipitation maximums have important implications for recharge to aquifers, particularly in urban environments. As the probability distribution of precipitation changes and possibly includes more intense events, LID and BMPs may play a critical role in capturing the runoff and promoting recharge that may otherwise overwhelm local storm water systems. Additional field and modeling studies are needed to measure LID performance under extreme weather [*Guo et al*., 2012] that is associated with ENSO and other climate variability.

[7] A better understanding of the capacity for managed recharge of storm water beneath LID is an important step toward the sustainable and conjunctive use of surface and groundwater resources in urban environments. Using results from a suite of methods to measure and model recharge beneath a recently installed (2009) LID BMP infiltration trench, this study addresses three main questions: (1) What are the benefits of measuring recharge using in situ methods compared to model-based and other simple estimates of recharge beneath a LID BMP? (2) What are recharge rates and volumes beneath the infiltration trench, how do they compare to an irrigated lawn that represents a non-LID source of urban recharge, and what are the important factors controlling recharge beneath the two sites? and (3) How effective is the LID BMP in capturing and recharging urban storm water considering historical ENSO variability and future climate change? This study provides the first field and model-based (HYDRUS-2D) [*Simunek et al*., 2008; *PC-Progress*, 2011] estimates of recharge rates and volumes beneath LID BMPs considering climate variability and change, and provides practical management information regarding enhanced storm water capture and recharge toward improved conjunctive use of water resources in urban environments.

2. Methodology

2.1. Study Area

[8] The study area is a recently installed (2009) and instrumented (2011) BMP infiltration trench and irrigated lawn site at the San Francisco State University (SFSU) LID research network, within the city of San Francisco, California, USA (Figure 1). Beneath SFSU is the Westside Basin aquifer (104 km^2), which is part of the regionally important California Coastal Basin aquifers (Figure 1). The Westside Basin aquifer system has a shallow (<30 m below sea level), unconfined aquifer and two deeper confined aquifers, and is bounded in the north and south by Franciscan Complex bedrock [*Clifton et al*., 1988; *Nzewi et al*., 2010]. The aquifer sediments include coastal deposits of sand, silt, mud, gravel, and peat from the Merced and Colma Formations. Based on a county-wide groundwater flow model, *Phillips et al*. [1993] reported 200 mm yr^{-1} as a spatially averaged estimate of natural and urban induced recharge to the Westside Basin aquifer. While the Westside Basin aquifer is not the primary source of drinking water for San Francisco, groundwater from the aquifer is used by a number of neighboring communities and saltwater intrusion from the San Francisco Bay has been a localized problem in the southeastern part of the aquifer [*Nzewi et al*., 2010].

[9] At the SFSU LID research network, a BMP infiltration trench was installed in 2009 and is approximately 11 m^2 (0.90 m × 12 m) in area and located in the center of a vegetated depression that collects runoff from an impervious bike path, parking lot, and surrounding roof tops with an effective drainage area of 430 m^2 (Figures 2a and 2b). The design of the infiltration trench follows the volume-based sizing method and a goal of 80% storm water volume capture [*California Stormwater Quality Association*, 2003] for 1 h, 6 h, and 24 h precipitation events (design storms) with a 2 year return interval. The irrigated lawn site (Figure 2c) is located approximately 300 m from the infiltration trench and was selected for this study as a representative source of urban recharge for comparison to the infiltration trench. The irrigated lawn site slope angle is near zero degrees and limits surface runon to the study site from surrounding vegetated areas, and thus the lawn site receives only direct precipitation and irrigation.

2.2. Vadose Zone Data Collection

[10] In May 2011, the infiltration trench and irrigated lawn were excavated, sediment cores were collected for

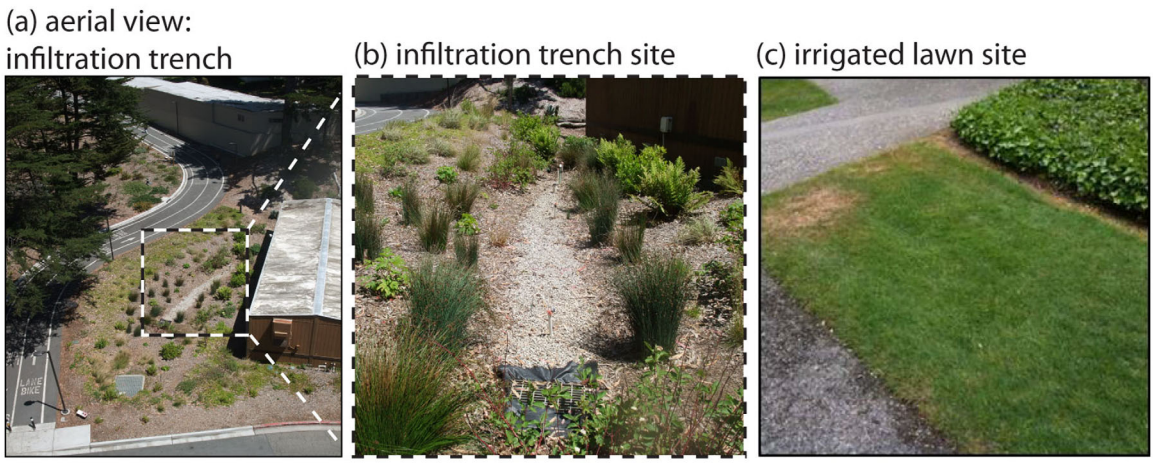

Figure 2. Photographs of the (a) infiltration trench from an aerial view, (b) infiltration trench, and (c) irrigated lawn sites at the San Francisco State University (SFSU) low impact development (LID) research network. The infiltration trench and irrigated lawn sites are separated by about 300 m.

sediment textural analysis and hydraulic properties, and instruments were installed to measure water content and matric potential and collect pore water from the vadose zone (Figure 3). The infiltration trench is filled with gravel that is 66 cm thick at the upstream end and thickens to 88 cm at the downstream end (Figure 3a). The gravel trench has an overflow drain with a 3.0 cm diameter weephole that discharges water to a storm drain when the trench reaches the maximum storage capacity of approximately 2.0 m^3 assuming a gravel porosity of 0.35. A total of six and five cores were collected beneath the infiltration trench (Figure 3a) and irrigated lawn (Figure 3b), respectively, and were analyzed for %sand, %silt, %clay, and %gravel by mass. We calculated bulk density ρ_b of the cores following the

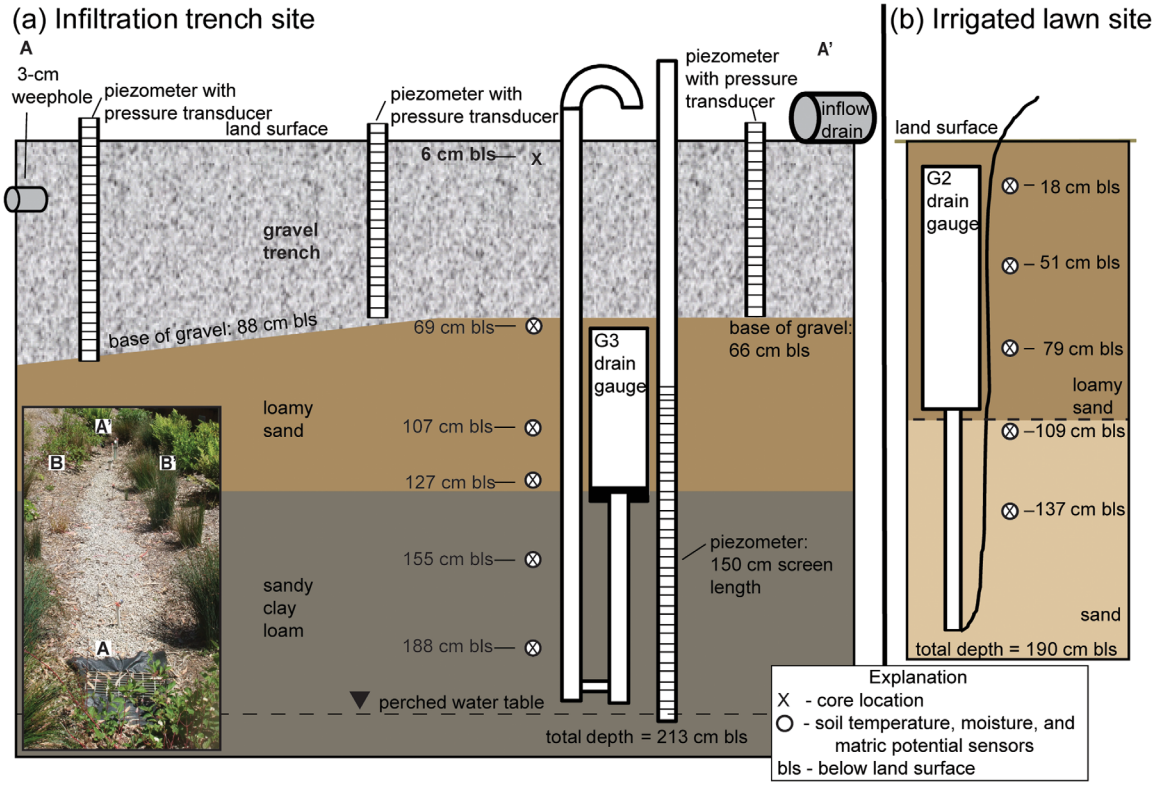

Figure 3. Schematic depiction (not to scale) of the instrumentation and core locations (a) along the longitudinal cross section A–A′ (inset) of the infiltration trench site and (b) beneath the irrigated lawn site, at the San Francisco State University (SFSU) low impact development (LID) research network. Lateral cross section B–B′ (inset) was used for the HYDRUS-2D model simulations.

Table 1. Soil Textural Class, Hydraulic Properties, and van Genuchten Fitting Parameters for Cores Collected at the Infiltration Trench and Irrigated Lawn Sites, and Corresponding Soil Layers Used in the HYDRUS-2D Models[a]

Core Depth (cm bls)	% Sand-Silt-Clay (by vol.)	% Gravel (by mass)	Soil Texture	θ_r ($m^3\ m^{-3}$)	θ_s ($m^3\ m^{-3}$)	α (m^{-1})	n	l (m^{-1})	K_s ($m\ d^{-1}$)	HYDRUS-2D Soil Layers (cm bls)
Infiltration Trench										
6	0-0-0	1.0×10^2	g	0.00	0.51	11	1.7	0.50	8.4×10^2	0–100
69	76-8.0-15	87	gsl	0.02	0.15	3.0	1.5	0.50	0.15	>100–106
107	86-2.0-11	0.30	ls	0.06	0.40	2.9	2.0	0.50	1.7	>106–108
127	84-4.0-11	0.80	ls	0.05	0.34	3.4	1.7	0.50	0.73	>108–127
155	64-8.0-27	8.6	scl	0.06	0.32	3.0	1.2	0.50	0.07	>127–155
188	64-8.0-27	20	scl	0.05	0.29	2.9	1.2	0.50	0.07	>155–188
Irrigated Lawn										
18	86-2.0-11	23	ls	0.05	0.29	2.9	1.9	0.50	1.0	0–18
51	88-2.0-9.0	1.0	ls	0.05	0.31	3.2	2.0	0.50	0.86	>18–51
79	88-2.0-9.0	0.40	ls	0.06	0.35	3.1	2.1	0.50	1.5	>51–79
109	88-2.0-9.0	0.20	ls	0.06	0.35	3.1	2.1	0.50	1.5	>79–109
137	92-2.0-5.0	1.2	s	0.05	0.34	3.2	2.7	0.50	3.0	>109–137

[a]bls, below land surface; vol., volume; g, gravel; gsl, gravelly sand loam; ls, loamy sand; scl, sandy clay loam; s, sand.

methods of *McMahon et al*. [2003], and used the program RETC [*van Genuchten et al*., 1991] to estimate residual θ_r and saturated θ_s volumetric content, saturated hydraulic conductivity K_s, and van Genuchten fitting parameters (α, n, l) (Table 1) for the water retention curves. We corrected the water content and hydraulic conductivity curves for the gravel content using the procedure outlined by *Bouwer and Rice* [1984]. The sediment texture and hydraulic properties were used in the HYDRUS-2D [*Simunek et al*., 2008; *PC-Progress*, 2011] simulations, as described below.

[11] Each site was instrumented with five Decagon 5TM soil temperature and moisture sensors, five Decagon MPS-1 matric potential sensors, and one Decagon G2 (or G3) drain gauge (Figure 3) that continuously record measurements at a 2 min interval to detect event-based changes in the vadose zone. The Decagon G3 drain gauge installed beneath the infiltration trench (Figure 3a) collects water volumes that must be extracted at daily intervals using a hand pump. The Decagon G2 at the irrigated lawn site (Figure 3b) uses an automated data logger and tipping bucket to measure water volume every 5 min, which is converted to a water flux [$L\ T^{-1}$] by dividing by area of the drain gauge. The sensors and drain gauge at the infiltration trench are approximately 1.0 m downgradient from the inflow pipe (Figure 3a). Additionally, one Decagon ECRN-100 rain gauge, one Solinst Inc. barometer, and three piezometers with Solinst Inc. pressure transducers were installed at the infiltration trench site (Figure 3a). The three piezometers were installed at the base of the gravel layer to measure standing water levels at approximately 1.0, 6.0, and 10 m downgradient from the inflow pipe (Figure 3a). A fourth piezometer with a 1.5 m screen was installed in the perched water table (2.1 m below land surface (bls)) at 1.0 m downgradient from the inflow pipe of the infiltration trench for manual water level measurements (Figure 3a). The Decagon sensors began collecting data on 19 June 2011, and the pressure transducers began collecting data on 4 January 2012.

2.3. Climate Variability

2.3.1. Historical Precipitation

[12] Historical daily precipitation data from the Mission Dolores station (CoopID 47772), San Francisco, CA (1914–2012) (Table 2) [*NOAA NCDC*, 2011; *WRCC*, 2012] were used to evaluate statistical differences in precipitation during El Niño and La Niña years and to estimate recharge rates and volumes beneath the infiltration trench and the irrigated lawn sites. Hourly precipitation data from the Mission Dolores station are available from 1948 to 2012 (Table 2). The hourly and daily precipitation data have mean values of 1.4 mm h^{-1} and 11 mm day^{-1} and maximum values of 45 mm h^{-1} and 1.4×10^2 mm day^{-1}, respectively, with the hourly and daily maximum values both on 23 January 1963. The Multivariate ENSO Index (MEI) (Figure 4) [*NOAA ESRL*, 2012; *NOAA*, 2012] was used to select years that were classified as being at least weak El Niño ($MEI > +0.6$) and La Niña ($MEI < -0.6$) events. The nonparametric Kruskall-Wallis test [*Helsel and Hirsch*, 2002; *Crawley*, 2007] indicates a statistically significant difference (p value = 0.04) between the daily precipitation during El Niño and La Niña years. The daily precipitation was aggregated to monthly totals, which generally indicate greater monthly precipitation during El Niño years and smaller monthly precipitation during La Niña years, particularly during winter months (Figure 5). We separated precipitation data sets into four categories for subsequent analyses: (1) 2011–2012 that represents the field observations at the LID BMP study site; (2) average historical (MEI between −0.6 and +0.6); (3) historical El Niño years; and (4) historical La Niña years.

Table 2. Summary Statistics for Hourly and Daily Precipitation at the Mission Dolores Station (CoopID 47772), San Francisco, CA, USA

Period of Record	1948–2012 (mm h^{-1})[a]	1914–2012 (mm d^{-1})[b]
Number of records	102,480	6646
Mean	1.4	11
Standard Deviation	1.7	10
Minimum	0.25	0.30
25th percentile	0.25	1.0
Median	0.76	7.9
75th percentile	1.8	11
99th percentile	8.1	47
Maximum	45	1.4×10^2

[a]Data source http://www.ncdc.noaa.gov/.
[b]Data source http://www.wrcc.dri.edu/.

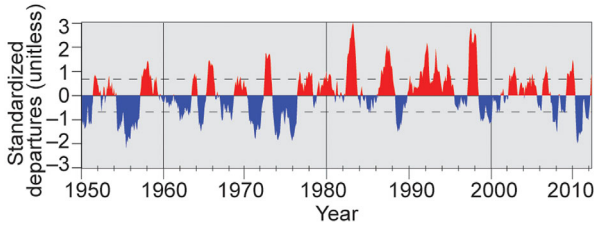

Figure 4. The monthly Multivariate El Niño Southern Oscillation (ENSO) index [*Wolter and Timlin*, 1993]. Red indicates the positive (warm) El Niño phase and blue indicates the negative (cold) La Niña phase of ENSO. The dashed line indicates years classified as being at least weak El Niño (MEI > +0.6) or La Niña (MEI < −0.6) events.

2.3.2. Future Precipitation Scenarios

[13] We used the NOAA Geophysical Fluid Dynamics Laboratory (GFDL) model [*NOAA GFDL*, 2012] and A1F1 (high emissions) scenario to evaluate one plausible response in recharge rates and volumes beneath the infiltration trench and the irrigated lawn sites to projected changes in the magnitude of precipitation events at the end of the 21st century (2099–2100). From among the many plausible 21st century climate sequences that might affect California, we selected the GFDL model because it has a relatively high sensitivity to greenhouse gas (GHG) forcings compared to the larger set of Intergovernmental Panel on Climate Change (IPCC) global climate models and because it has been used successfully in previous studies of climate change in California [*Cayan et al*., 2006, 2008]. Most importantly for the goals of evaluating the effects of future ENSO variability on recharge, the GFDL model projections of precipitation exhibit considerable interannual variability that is significantly related to ENSO [*Cayan et al*., 2006, 2008]. The A1F1 scenario represents a world that remains reliant on fossil fuels, leading to a best-estimate temperature rise of 4.0°C from 1990 levels by 2100 [*IPCC*, 2007]. Percent change in future precipitation was calculated by month between the GFDL 21st century A1F1 and GFDL 20th century model using the delta-change downscaling method, as described next.

[14] We used the comparatively cheap and computationally efficient delta-change downscaling method [*Fowler et al*., 2007; *Taylor and Tindimugaya*, 2012] to generate a predicted local San Francisco precipitation data set from the large spatial scale (1° latitude–1° longitude) GFDL data. The delta change (%) is calculated for each month, but the delta change (%) is applied to the hourly and daily precipitation for the corresponding month from the local San Francisco data set. This monthly delta-factor method is more detailed than some previous studies that calculate and apply a single percentage change to all precipitation throughout the year [*Barbu et al*., 2008; *Pyke et al*., 2011]. The method assumes a similar frequency and timing of events between historical and future precipitation and only accounts for future changes in the mean, maxima, and minima of precipitation events, which is most relevant for the heavily urbanized study area and for evaluating LID recharge efficiency. Summary statistics were calculated for the GFDL 20th century and the 21st century A1F1 precipitation data and then analyzed by month using a Kruskall-Wallis test [*Helsel and Hirsch*, 2002; *Crawley*, 2007].

[15] Using a linear mixed-effects model (LME) [*Crawley*, 2007], we evaluated the forecasted net precipitation difference between the GFDL 21st and 20th century to identify statistically significant changes in future precipitation. An LME model is more appropriate than other linear models because it accounts for temporal pseudoreplication, which is a characteristic of monthly to seasonal variability in meteorological data such as precipitation [*Crawley*, 2007]. The LME model also accounts for fixed and random effects; time is the explanatory variable and the data are analyzed with and without the time variable as a fixed and random effect [*Crawley*, 2007]. To evaluate the effect of time on the overall trend in simulated precipitation, we ran the LME model using three different scenarios: (1) time as a fixed effect; (2) time as a fixed effect and random effect; and (3) time only as a random effect. An ANOVA analysis was subsequently run on the output from the three LME model scenarios to determine which model produces the best fit regarding the statistical significance of time as a predictor of change in simulated precipitation [*Helsel and Hirsch*, 2002; *Crawley*, 2007].

2.4. Recharge

[16] Recharge is the vertical flux of water across the water table and is expressed as volume per time [$L^3\ T^{-1}$] or more commonly as length per time [$L\ T^{-1}$]. We estimate recharge using the following methods: (1) Darcy method; (2) in situ drainage; (3) HYDRUS-2D; and (4) water budget.

2.4.1. Darcy Method

[17] Recharge rates were estimated using the one-dimensional Darcy method [*Healy*, 2010]:

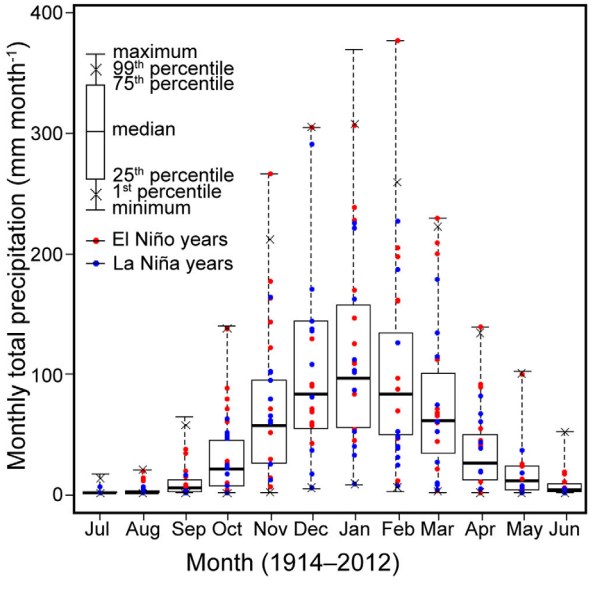

Figure 5. Distribution of precipitation (mm) by month at the Mission Dolores station (CoopID 47772), San Francisco, California from 1914 to 2012. El Niño and La Niña years (1952–2012) from the Multivariate El Niño/Southern Oscillation (ENSO) Index (MEI) [*NOAA*, 2012] are indicated.

$$R = K_s \cdot K_r(h) \cdot \frac{\partial H}{\partial z} \quad (1)$$

where R is recharge [L T^{-1}], K_s is the vertical saturated hydraulic conductivity [L T^{-1}], $K_r(h)$ is the unsaturated hydraulic conductivity coefficient at the ambient pressure head, h; H is total head [L]; and z is depth bls [L]. All input values were derived from the previously described field instrumentation and from water retention curves built from a sediment textural analysis of the sediment cores (Table 1).

2.4.2. In Situ Drainage

[18] We collected the drainage volume [L^3] from the G3 drain gauge beneath the infiltration trench on an approximate daily schedule. The daily drainage volume was converted to a flux [L T^{-1}] by dividing by the area of the drain gauge (471 cm^2) and one day. At the irrigated lawn site, the G2 drain gauge records a water drainage flux every 5 min with a data logger. Based on the total-potential profile and downward hydraulic gradient measured at each site, described below, we assume that water collected in the drainage gauge beneath the infiltration trench and irrigated lawn is representative of recharge.

2.4.3. HYDRUS-2D

[19] We estimated recharge rates using a HYDRUS-2D numerical model [*Simunek et al*., 2008; *PC-Progress*, 2011]. HYDRUS-2D solves the Richards equation [*Richards*, 1931] for saturated and unsaturated water flow and Fickian-based advection-dispersion equations for heat and solute transport [*Simunek et al*., 2008].

[20] The HYDRUS-2D model domain was constructed using a 2.4 m high × 3.0 m wide lateral cross section of the infiltration trench (Figure 3a) with 63,000 2D-finite elements and a mesh size of 0.03 m. The HYDRUS-2D mesh was designed to capture the intrinsic changes that occur at soil boundaries by reducing the mesh size to 0.01 m at soil boundaries, which is especially important at the gravel-sand boundary at the infiltration trench site. A 2.0 m × 2.0 m model domain was used for the irrigated lawn, which has 45,000 2D-finite elements and the same 0.03 m mesh size as the infiltration trench. Based on the textural analyses from the sediment cores, six and five soil layers were used in the infiltration trench and irrigated lawn model domains, respectively (Table 1).

[21] The HYDRUS-2D models for the infiltration trench and irrigation lawn were initialized to steady state using constant head boundary conditions for 50 days. The infiltration trench model was initialized with a constant upper-head boundary of −0.94 m and a constant bottom-head boundary of −0.20 m with pressure head increasing linearly with depth representing values obtained from the field matric potential sensors. The irrigated lawn model was initialized with a constant upper-head boundary of −0.90 m and a constant bottom-head boundary of −0.50 m. Steady-state runs were initialized for both models at a minimum time step of 1 s. The output pressure head field was then used as initial conditions for the transient simulations.

[22] Recharge was then estimated by running transient precipitation scenarios and averaging the volumetric flux at the bottom of the model domain for each year. A 1 year transient simulation with an hourly time-discretization was run for the infiltration trench using precipitation, runoff, evaporation, and irrigation (as described below) as time-variable parameters for the year 2011–2012. A similar 1 year transient simulation was run for the irrigated lawn at a daily time-discretization to reduce model run-times and using precipitation, irrigation, soil evaporation, and evapotranspiration (also described below) for the time-variable conditions. The model calibration was evaluated at a daily time step by comparing simulated recharge (mm) to observed recharge (mm) ($N = 25$) from the in situ drain gauge between October 2011 and March 2012 and was within acceptable levels of performance criteria [*Moriasi et al*., 2007] for the infiltration trench (Nash-Sutcliffe efficiency (NSE) = 0.1; root-mean-square error (RMSE) = 61 (mm)) and the irrigated lawn (NSE = 0.6; RMSE = 7.0 (mm)) models. Simulated daily recharge rates from the calibrated models were evaluated against an independent set ($N = 12$) of observed recharge (mm) from the in situ drain gauge and was within acceptable levels of performance criteria [*Moriasi et al*., 2007] for the infiltration trench (NSE = 0.3; RMSE = 38 (mm)) and the irrigated lawn (NSE = 0.9; RMSE = 6.0 (mm)) models. The infiltration trench and irrigated lawn models tended to overestimate recharge during the winter and spring likely because of overestimating the actual irrigation input, assumptions of homogeneity of hydraulic properties within the simulated soil layers, and underestimating actual runoff from the irrigated lawn. During the summer and fall, the models tended to underestimate recharge likely because of uncertainties in the actual ET, particularly during the foggy summer months in San Francisco. Transient simulations from the calibrated models of the infiltration trench and irrigated lawn were run with future predicted precipitation, based on the linearly transformed Mission Dolores station data set and runoff values for the end of the 21st century (year 2099–2100).

2.4.4. Water-Budget Method

[23] We used the water-budget method [*Healy*, 2010] to estimate recharge beneath the infiltration trench and the irrigated lawn sites by incorporating precipitation, irrigation, evaporation, transpiration, runoff from impermeable surfaces, and changes in storage. Details of the water-budget method are available in supporting information.

[24] Using the water-budget method, we define recharge efficiency (%) as the percentage of total water inputs to the infiltration trench or irrigated lawn that becomes recharge:

$$\text{Recharge efficiency } (\%) = \frac{\text{Inputs} - \text{Outputs}}{\text{Inputs}} \times 100 \quad (2)$$

where the inputs (precipitation P, runoff R_{off}, and irrigation I) and the outputs (overflow O_f and evapotranspiration ET) are described in supporting information (equation (SI-1)). At the irrigated lawn site, the only inputs are P and I. We calculated the annual recharge efficiency for each of the four recharge methods and for the El Niño and La Niña years between 1954 and 2012 in order to evaluate the performance of the infiltration trench in capturing storm water runoff and enhancing recharge.

3. Results

3.1. Water Movement and Storage in the Vadose Zone

[25] Daily time series of total (matric plus gravimetric) potentials in the vadose zone beneath the infiltration trench

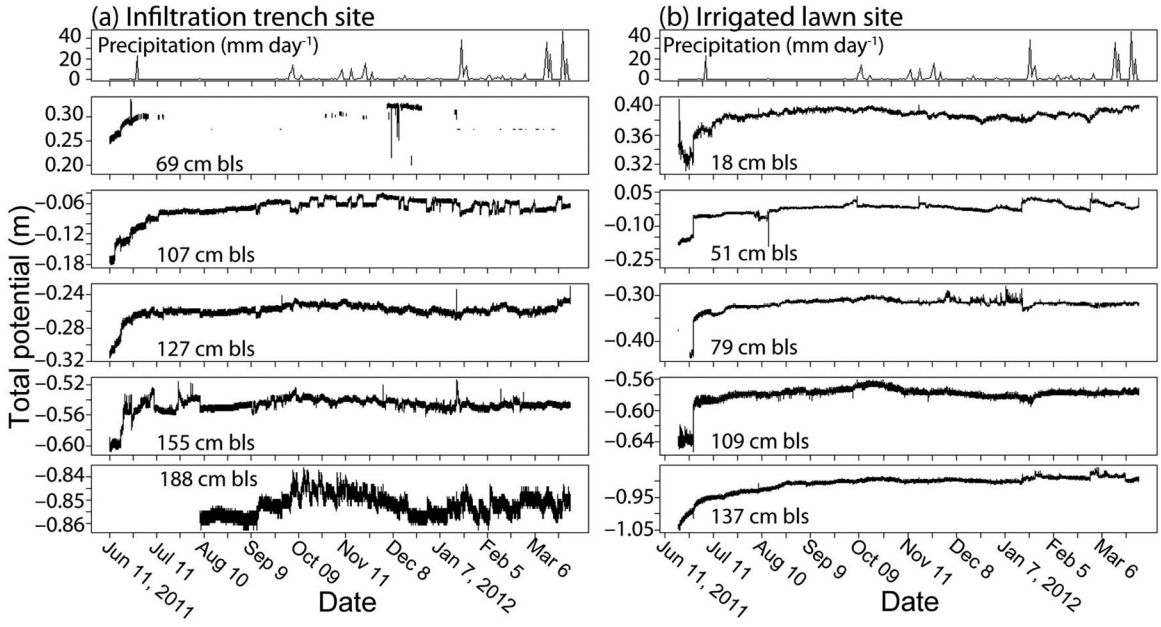

Figure 6. Daily time series (June 2011 to March 2012) of precipitation (mm d^{-1}) and total (matric plus gravimetric) potential (m) for depths below land surface (bls) at the (a) infiltration trench site and (b) irrigated lawn site.

and irrigated lawn are shown in Figure 6. The total potentials indicate that most of the Decagon MPS-1 matric potential sensors required 1–2 weeks to reach equilibrium with the native sediments. After this initial equilibrium period, the total potential value remained relatively constant at most of the depths beneath the infiltration trench (Figure 6a) and irrigated lawn (Figure 6b) sites. The lack of measurements from the sensor at 69 cm bls (3.0 cm below the gravel) likely indicates that the matric potential values were out of measurement range because this soil layer was saturated by water infiltrating beneath the trench (Figure 6a).

[26] The sensors deeper in the profile at 107, 127, and 155 cm bls (41, 61, and 89 cm below the gravel) show no appreciable fluctuations until precipitation events in fall (September–November) 2011 (Figure 6a). The total potential response to the fall precipitation events is less apparent beneath the irrigated lawn (Figure 6b) due to the daily irrigation that keeps the matric potential values near saturated conditions and apparently dampens changes in the total potential due to precipitation events. The substantial precipitation events in January 2012 resulted in a sharp and discrete increase in total potentials at all depths beneath the infiltration trench (Figure 6a) and a more damped increase at depths beneath the irrigated lawn (Figure 6b), which likely indicates the propagation of a wetting front and discrete recharge events beneath both sites. The variations in the total potentials at the bottom of the infiltration trench profile (sensor at 188 cm bls) (Figure 6a) are likely the response to recharge events causing fluctuations in the perched water table at approximately 213 cm bls.

[27] Selected total-potential profiles on three representative days in the comparatively drier summer and wetter fall and spring months show a monotonic decrease in total potential with depth, indicating a predominantly downward hydraulic gradient beneath the infiltration trench (Figure 7a) and irrigated lawn (Figure 7b). The observed total-potential profiles approach unit gradient ($d\mathrm{H}\ dz^{-1} = -1.00$) beneath the infiltration trench (-1.01 m m^{-1}) and the irrigated lawn (-1.02 m m^{-1}) and indicate a constant downward flux of water driven by gravity beneath both sites [*Healy*, 2010]. The constant downward hydraulic gradient and flux are likely controlled by the water storage capacity of the gravel trench and the irrigation at both sites and are similar to gradients beneath some irrigated agricultural fields, such as in the High Plains aquifer [*McMahon et al*., 2003; *Gurdak et al*., 2007]. Unlike the nonirrigated lands in the High Plains [*Gurdak et al*., 2007], the total-potential profiles here indicate no upward hydraulic gradients at either the infiltration trench or irrigated lawn. Although the total-potential profile beneath the irrigated lawn is systematically more negative (drier conditions) during the summer than fall-spring (Figure 7b), the downward hydraulic gradient is maintained throughout the year.

[28] Compared to the temporal variations in total potential (Figure 6), there is considerably more variability in the daily time series of volumetric water content beneath the infiltration trench (Figure 8a) and irrigated lawn (Figure 8b). As expected, the daily time series of volumetric water content with depth capture similar event-based responses as the total potential time series. Substantial increases in volumetric water content occur at all depths beneath the infiltration trench in response to the precipitation in fall 2011 and particularly winter 2012 (Figure 8a), and indicate recharge events in response to the precipitation. Although variability in volumetric water content is less beneath the irrigated lawn (Figure 8b) compared to the infiltration trench, event-based wetting fronts occur in fall 2011 and winter 2012 in response to the same precipitation events as at the infiltration trench site. The variability in volumetric water content

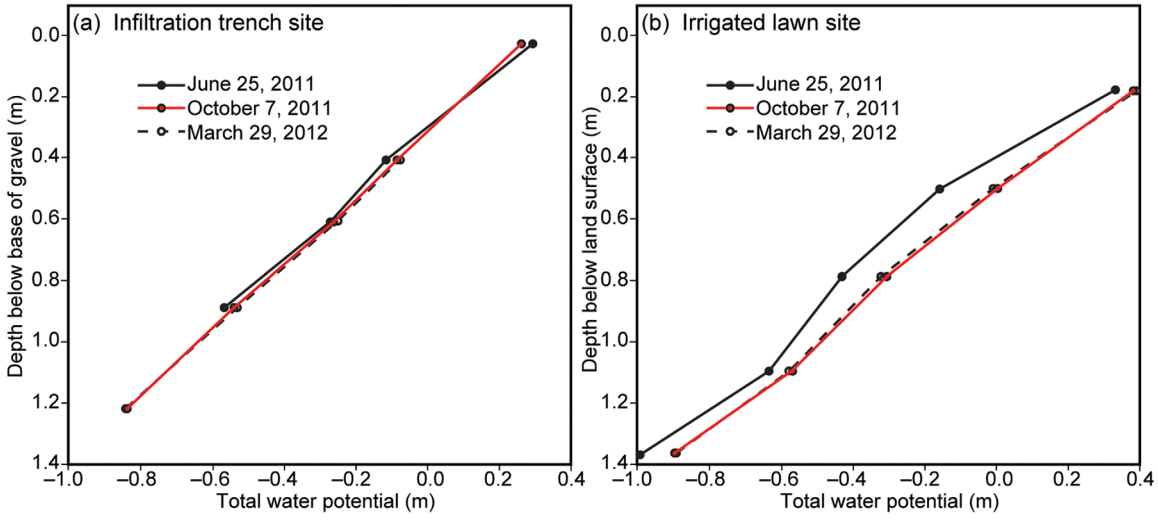

Figure 7. The approximate steady state total-potential profiles approach unit gradient ($dH\,dz^{-1} = -1.00$) and indicate a constant downward flux of water beneath the (a) gravel at the infiltration trench and (b) land surface at the irrigated lawn as shown for selected days during the comparatively drier summer (25 June 2011) and wetter fall (7 October 2011) and spring (29 March 2012) months (Figure 4).

beneath the irrigated lawn during summer 2011 is a response to daily irrigation and not precipitation.

[29] Volumetric water content profiles for selected infiltration events during June–July and September 2011 indicate important differences in water redistribution and storage beneath the infiltration trench (Figure 9a) and irrigated lawn (Figure 9b). The volumetric water content generally increases with depth beneath the infiltration trench, which is a result of the perched water table maintaining near saturated conditions at the base of the profile (Figure 9a). The volumetric water content beneath the irrigated lawn decreases with depth and the daily irrigation maintains relatively high volumetric water content at the top of the profile (Figure 9b). The redistribution of water beneath the infiltration trench, as demonstrated for selected wetting (11 June and 15 September 2011) and drying (11 July and 22 September 2011) cycles (Figure 9), is much more complex than beneath the irrigated lawn. Based on the observed total-potential gradients and constant downward hydraulic gradients (Figure 7), the redistribution of water is continuously downward and eventually becomes recharge. The observed range (June 2011 to March 2012) in volumetric water content profiles and corresponding water storage is much greater beneath the infiltration trench than beneath the irrigated lawn. In fact, the minimum water storage beneath the infiltration trench is 0.29 m (maximum = 0.51 m) and is nearly greater than the maximum of 0.31 m (minimum = 0.27 m) water storage beneath the irrigated lawn (Figure 9). The downward hydraulic gradients and substantially larger water storage in the vadose zone are evidence for larger recharge rates beneath the infiltration trench than the irrigated lawn.

3.2. Future Precipitation

[30] The results of the LME model applied to the GFDL A1F1 precipitation data indicate a net decrease of 0.14 mm day^{-1} from 1861 to 2100. ANOVA analysis on the three

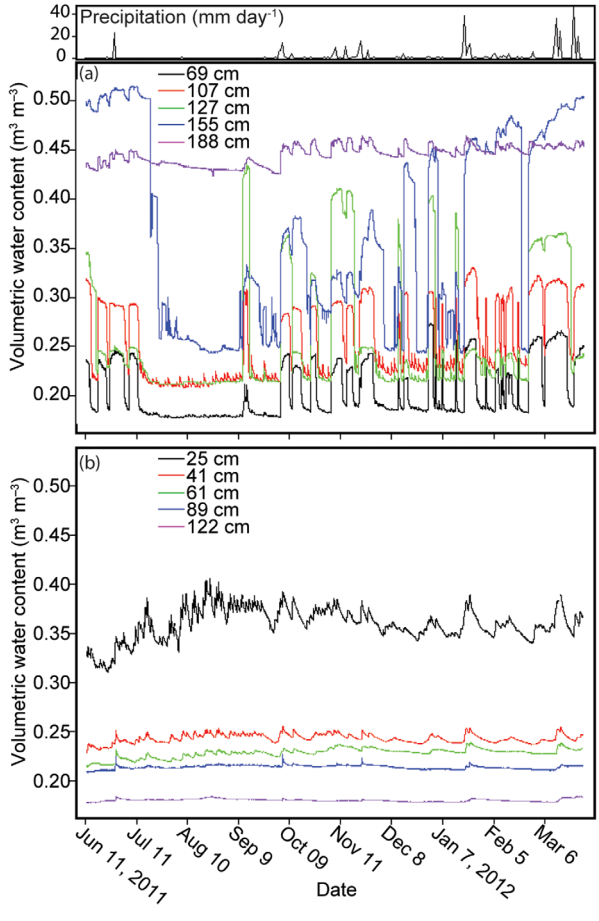

Figure 8. Daily time series (June 2011 to March 2012) of precipitation (mm d^{-1}) and volumetric water content (m^{-3} m^{-3}) from the five Decagon 5TM soil moisture sensors beneath the (a) gravel at the infiltration trench site and (b) land surface at the irrigated lawn.

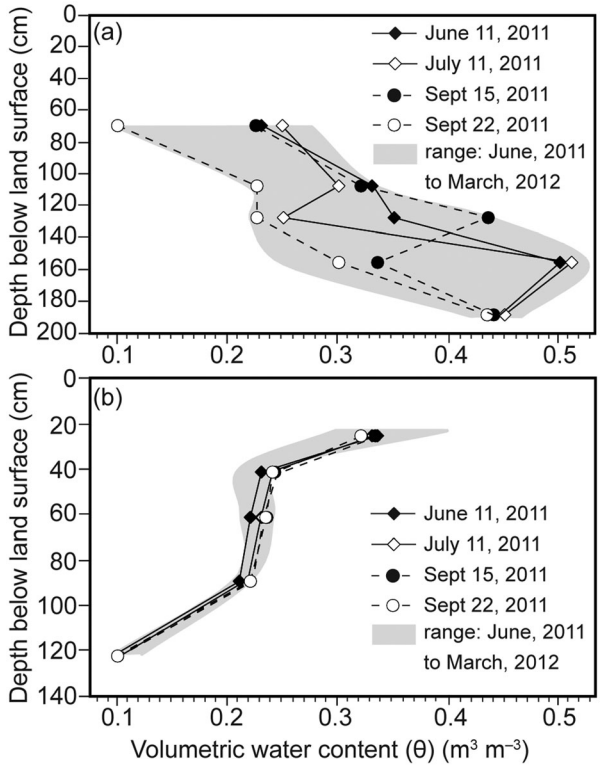

Figure 9. Volumetric water content profiles beneath the (a) infiltration trench and (b) irrigated lawn indicate redistribution stages for selected wetting and drying cycles in response to precipitation in June and September 2011. Water storage ranges from 0.29 to 0.51 m beneath the infiltration trench and from 0.27 to 0.31 m beneath the irrigated lawn.

LME models (with and without fixed and random effects) indicates that the decrease of 0.14 mm day^{-1} from 1861 to 2100 is not statistically significant ($p = 0.72$) at the α level = 0.05. When accounting for time as a random and fixed effect, there is no apparent statistical evidence to support an increasing or decreasing trend in total daily precipitation in San Francisco over the 21st century with the GFDL A1F1 scenario. Similar findings are reported by *Pierce et al*. [2012] whose use of ensemble GCM forecasts indicate near 0.0% change in mean annual precipitation for parts of northern California by the 2060s. However, we find that the percent change in historical (1861–2000) and 21st century (2000–2100) daily precipitation, when separated by month, is statistically significant (α level = 0.05, Kruskall-Wallis test) for 10 months of the year (Table 3). Only February and March are forecast by the GFDL A1F1 model to have no statistically significant change in daily precipitation over the 21st century (Table 3). When aggregated by season, the 21st century daily precipitation is forecast to change by +8.0%, −8.0%, −19%, and −6.0% for winter (DJF), spring (MAM), summer (JJA), and fall (SON), respectively. These forecast seasonal changes have similar sign and magnitude as those findings by *Pierce et al*. [2012] that indicate seasonal changes in San Francisco precipitation for the 21st century of +2.0%, −18%, −15%, and −5.0% for winter, spring, summer, and fall, respectively. Compared to *Pierce et al*. [2012], our results are nearly identical during fall, but overestimate winter and spring precipitation and underestimate summer precipitation. The San Francisco area is drier in the summer (Figure 5), so the difference in percentage change during that time of year represents small amounts of precipitation that are not as important in terms of recharge beneath LID BMPs. Therefore, our forecast future precipitation from the LME downscaling from the single GFDL model are comparable estimates of future precipitation patterns to those forecasts by *Pierce et al*. [2012] using a more complex and unbiased statistical and dynamic spatial downscaling approach from an ensemble of 16 GCMs with the SRES A2 emission scenario. Additionally, we evaluated the forecast changes for low (<8.0 mm) and high (>8.0 mm) intensity, 24 h duration storm events between the GFDL 20th century data set and the GFDL A1F1 21st, and note that the low intensity 24 h events are predicted to decrease by −3.2% ($p = 0.04$), while high intensity 24 h events are predicted to increase by +11% ($p < 0.01$). These results are consistent with recent (2013) findings of statistically significant changes in the frequency and magnitude of extreme precipitation events over the historical record across the San Francisco Bay area [*Russo et al*., 2013].

3.3. Recharge Rates and Volumes

[31] Recharge rates and volumes beneath the infiltration trench and irrigated lawn as calculated using the Darcy, In situ, HYDRUS-2D, and water-budget methods are shown in Table 4. The estimated recharge rates are an order of magnitude greater beneath the infiltration trench (1750–3710 mm yr^{-1}) than beneath the irrigated lawn (130–730 mm year^{-1}) (Table 4), which is consistent with the observed differences in water storage beneath the two sites and the larger volume of runoff entering the infiltration trench. Except for recharge rates calculated beneath the irrigated lawn using the in situ drainage and water-budget methods, all rates are substantially greater than the 200 mm yr^{-1} natural and urban induced recharge rate reported by *Phillips et al*. [1993]. The HYDRUS-2D 2099–2100 simulated recharge rate beneath the infiltration trench is 3710 mm yr^{-1}, which is 1130 mm more than HYDRUS-2D 2011–2012 simulated annual recharge (2580 mm yr^{-1}) (Table 4). We attribute the substantial difference in

Table 3. Daily Historical and Predicted Precipitation From the GFDL A1F1 Scenario and Percent Change by Month

Month	Historical (1861–2000) (mm day^{-1})	Predicted (2000–2100) (mm day^{-1})	Percent Change	Kruskall-Wallis p Value
Jan	9.6	11	24%	<0.01
Feb	8.8	9.0	2.9%	0.31
Mar	5.6	6.2	11%	0.73
Apr	3.6	2.7	−25%	<0.01
May	2.2	1.9	−11%	<0.01
Jun	1.3	1.4	12%	<0.01
Jul	2.0	1.0	−49%	<0.01
Aug	2.4	1.9	−21%	<0.01
Sep	4.1	3.8	−8.0%	<0.01
Oct	4.5	4.7	3.4%	0.05
Nov	6.2	5.3	−14%	<0.01
Dec	8.8	8.5	−3.1%	<0.01

Table 4. Calculated Annual Recharge Rates, Volumes, and Efficiencies Beneath the Infiltration Trench and Irrigated Lawn

Method	Period	Inflow volume (m^3 yr^{-1})	Recharge rate (mm yr^{-1})	Recharge volume (m^3 yr^{-1})	Recharge efficiency (%)
Infiltration Trench Site					
1D-Darcy	2011–2012	33	2340	25	76
In situ drainage	2011–2012	33	1750	19	58
HYDRUS-2D	2011–2012	36	2580	28	78
HYDRUS-2D	2099–2100	52	3710	41	79
Water budget	2011–2012	33	1960	21	64
Irrigated Lawn Site[a]					
1D-Darcy	2011–2012	667	510	220	33
In situ drainage	2011–2012	667	130	56	8.0
HYDRUS-2D	2011–2012	674	410	176	26
HYDRUS-2D	2099–2100	1070	730	312	29
Water budget	2011–2012	667	180	75	11

[a]Volume calculated using a hypothetical area = 430 m^2, which is the drainage area of the infiltration trench. Irrigation accounts for 76% of the total water input to the irrigated lawn.

simulated historical and future recharge rates to the relatively lower annual recharge in 2011–2012, which was a La Niña year. As discussed below, the HYDRUS-2D 2099–2100 simulated recharge rate is within the range simulated when considering interannual El Niño and La Niña variability in precipitation. Although the recharge rates are substantially greater beneath the infiltration trench, the estimated recharge volume is generally an order of magnitude smaller beneath the infiltration trench (19–41 m^3) than the irrigated lawn (56–312 m^3) with a similar drainage area (430 m^2) (Table 4). This inconsistency between recharge rates and volumes beneath the two sites is addressed in section 4.

3.4. ENSO Variability and LID Recharge Rates and Efficiency

[32] The water-budget based estimates of annual recharge rates beneath the infiltration trench as a function of El Niño and La Niña precipitation variability between 1954 and 2012 are shown in Figure 10a. These recharge rates range from 1390 to 5840 mm yr^{-1} and average 3410 mm yr^{-1} for El Niño years, and range from 1540 to 3330 mm yr^{-1} and average 2430 mm yr^{-1} for La Niña years. The substantial difference in recharge rates between El Niño and La Niña years is largely a function of the difference in annual precipitation, which is generally less than about 700 mm yr^{-1} during La Niña years but can exceed 800 mm yr^{-1} during El Niño years (Figure 10a). Figure 10a indicates that the total annual precipitation can be used to estimate annual recharge rates beneath the infiltration trench with reasonably good predictive ability ($r^2 = 0.92$). However, total annual precipitation is a poor predictor of recharge efficiency beneath the infiltration trench (not shown), possibly because of uncertainties in the estimated water budget inputs and outputs. Based on the El Niño and La Niña precipitation variability between 1954 and 2012, estimated recharge efficiency beneath the infiltration trench varies between 35 and 70% and has a moderately correlated ($r^2 = 0.36$), inverse relation to the maximum annual precipitation intensity (mm) for 24 h duration storm events during El Niño and La Niña years between 1954 and 2012 (Figure 10b). The estimated recharge efficiencies between 1954 and 2012 are also considerably less than the recharge efficiencies (58–79%) for the current (2011–2012) and future (2099–2100) periods (Table 4).

4. Discussion

4.1. Benefits of In Situ LID Recharge Measurements

[33] We estimated recharge rates and volumes using two in situ methods (1D-Darcy method and in situ drain gauge) and two models (HYDRUS-2D and water-budget method). Considering the period of observation only, recharge rates

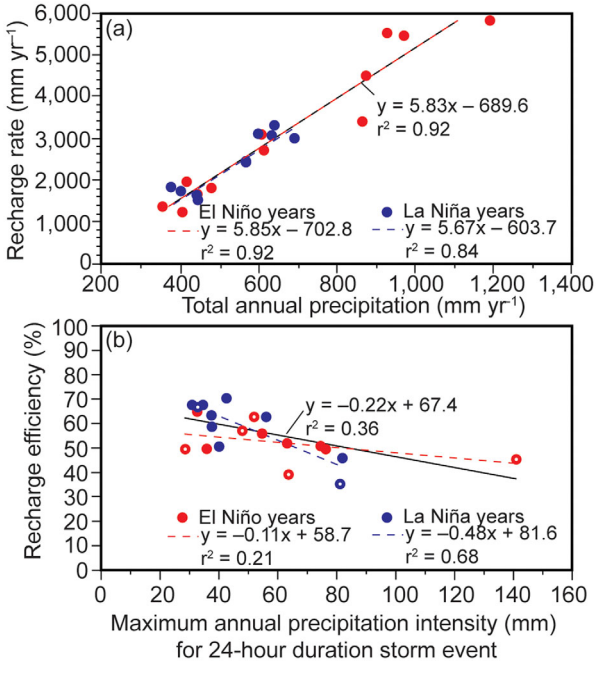

Figure 10. Annual water budgets for the infiltration trench during El Niño and La Niña years between 1954 and 2012 indicate that (a) recharge rates (mm yr^{-1}) are strongly correlated ($r^2 = 0.84$–0.92) to total annual precipitation (mm yr^{-1}) and (b) recharge efficiency (%) is weakly to moderately correlated ($r^2 = 0.21$–0.68) to the maximum annual precipitation intensity (mm) for a 24 h duration storm event. The El Niño and La Niña years with the inner white dots have 1 hour precipitation events that exceed the 5 year design storm.

and volumes ranged between 1750–2340 mm yr^{-1} and 19–25 m^3 yr^{-1} for the in situ methods and were generally consistent with the range of 1960–2580 mm yr^{-1} and 21–28 m^3 yr^{-1} estimated using the models (Table 4). Although the in situ methods are more applicable than the models for monitoring individual recharge events and providing insight into the mechanics of the recharge process, the models can also be used to estimate recharge and identify important processes during historical and future periods where in situ observations are not available.

[34] Each of the four methods is subject to errors that propagate through the calculations and cause uncertainty in the recharge estimates. Errors are introduced in the 1D-Darcy method by the limitations in accurately quantifying the variability in the hydraulic gradient and unsaturated hydraulic conductivity [*Healy*, 2010]. At our field sites, the five Decagon MPS-1 sensors at each site generate high spatial and temporal resolution hydraulic gradient profiles that reduce uncertainty and support our assumption of using the unit hydraulic gradient to simplify the 1D-Darcy method. Another advantage of continuously measuring matric (total) potentials is to identify zero-flux planes ($dH\ dz^{-1} = 0.0$) and total potential profiles that indicate upward hydraulic gradients, which are possible beneath LID in more semiarid and arid environments. Not identifying upward hydraulic gradients during periods of low or no rainfall could lead to inaccuracies in the underlying conceptual model, serious errors in a water budget or other model-based methods, and possibly result in overestimating the actual recharge beneath the LID BMP.

[35] Recharge rates beneath the infiltration trench and irrigated lawn are generally greater using the 1D-Darcy method (2340 and 510 mm yr^{-1}) compared to the in -situ drainage rates (1750 and 130 mm yr^{-1}) (Table 4). The smaller recharge rates from the in situ drain gauge may be attributed to the repacking of native sediments during installation that artificially increase the soil bulk density and decrease porosity and hydraulic conductivity in the drain gauge. A single drain gauge may not capture spatial infiltration patterns beneath all LID BMPs, but the installation of our drain gauge near the inflow drain (Figure 3) helps to ensure that a large component of inflow is measured by the drain gauge. Most importantly, the in situ methods provide data that are needed to calibrate the models and verify simulated recharge estimates.

[36] The recharge rates estimated beneath the infiltration trench using the HYDRUS-2D (2011–2012) model and 1D-Darcy method (Table 4) are similar and within 240 mm yr^{-1} (<10%) of each other. Due to simplifying assumptions and model convergence problems with HYDRUS-2D (2011–2012), some time-varying precipitation boundary conditions had to be spaced out over longer time periods (a few hours in some cases) than the actual storm duration, which likely accounts for the higher recharge rates using HYDRUS-2D (2011–2012) than the water-budget and in situ methods. Future models may more accurately capture storm events by using a time discretization of minutes instead of hours. As with any numerical model, the HYDRUS-2D is one representation of the real system and inherently introduces uncertainty in the recharge estimate. Building and calibrating the HYDRUS-2D model also requires a greater time investment than the other methods. However, a benefit of a well calibrated HYDRUS-2D model is the ability to simulate hourly or event-based recharge rates that may not be possible using a water-budget method, and to simulate future scenarios (2099–2100 in our study) that may be invaluable during the design, maintenance, and operation of LID BMPs under present climate variability and during urban planning for adaptation and resilience under future climate change.

[37] Compared to the HYDRUS-2D model, the water-budget method requires less of a time investment to generate recharge estimates that are most relevant on time scales from weeks to years because some inflows, outflows, and change in storage values used in the water budget are not available or have considerable uncertainty at the event time scales (<day). However, the magnitude of the water-budget inflow, outflow, and change in storage components directly affects the uncertainty that each components contributes to the overall uncertainty of the recharge estimate [*Healy*, 2010]. The larger magnitude inflow components of precipitation and runoff and smaller magnitude irrigation inflows are well constrained from the onsite precipitation gauge, TR-55 SCS curve number method, and automatic sprinkler irrigation control. Although the outflow components of overflow (O_f, equation (SI-1)) and evapotranspiration (ET, equation (SI-1)) likely have more uncertainty than the inflows, O_f and ET are much smaller in magnitude than the inflows and thus have a smaller affect on the overall uncertainty of the recharge estimates. The overflow is a function of the maximum storage capacity of the gravel trench, which is estimated at 2.0 m^3 based on geometry of the trench and assuming a gravel porosity of 0.35. The estimated gravel porosity of 0.35 is inherently uncertain and is likely to decrease with time as pore spaces fill with silt from the runoff.

4.2. Comparison of Recharge Beneath the Infiltration Trench and Irrigated Lawn

[38] Recharge rates are substantially greater beneath the infiltration trench compared to the irrigated lawn (Table 4). Because the infiltration trench collects water from a larger area, to compare recharge volumes beneath the infiltration trench and irrigated lawn we need to consider an equal catchment area. The estimated recharge volume is generally an order of magnitude greater beneath an area of irrigated lawn (56–312 m^3) with similar area as the drainage area (430 m^2) of the infiltration trench (19–41 m^3) (Table 4). Similarly, the previously reported 200 mm yr^{-1} natural and urban induced recharge by *Phillips et al*. [1993] applied to 430 m^2 is 86 m^3 recharge volume, which is also substantially greater than the estimated recharge volume beneath the irrigated trench. This somewhat counterintuitive finding of less recharge volume beneath the infiltration trench than the irrigated lawn is a function of the smaller inflow volumes to the infiltration trench (33–52 m^3) than the irrigated lawn (667–1070 m^3) (Table 4).

[39] Although the recharge efficiencies reported here (58–79%, Table 4) are somewhat lower than the previously reported range of 40–98.8% [*Dietz*, 2005; *Dietz and Clausen*, 2006; *Ermilio and Traver*, 2006; *Endreny and Collins*, 2009; *Stephens et al*., 2012], the recharge efficiency beneath the infiltration trench is substantially greater than beneath the irrigated lawn (8.0–33%, Table 4), even

considering the much lower inflow to the infiltration trench than the irrigated lawn. The storage capacity of the gravel trench enables more efficient infiltration and recharge of storm water that would otherwise runoff, as highlighted by the low recharge efficiencies of the excess irrigation water at the irrigated lawn site.

[40] We demonstrate a clear benefit for recharge and local groundwater resources using small, spatially distributed storm water retention BMPs such as infiltration trenches. Our findings support other studies that recommend the use of LID BMPs. For example, *Devinny et al*. [2005] suggest that using BMPs in the Los Angeles, California region to comply with federal and state surface-water quality regulations could have an estimated benefit of additional groundwater supplies that have a 2005 value of $7.2 billion. Additionally, smaller-scale, spatially distributed BMPs such as the infiltration trench in this study may be used to help supplement conventional and more costly managed-aquifer storage and recovery (MAR) projects that use larger-scale surface spreading basins and injections wells. The increased recharge and groundwater storage beneath small scale, distributed BMPs may also help to increase groundwater discharge to gaining streams and wetlands and create longer baseflow periods that help support and improve important ecological services and functions. The potential downside of BMPs that enhance recharge, particularly in urban environments, is the potential for flooding of basements, foundations, and subsurface transportation infrastructure. Therefore, the cost-benefit of such BMPs is greater in semiarid and arid climate regions where the depths to water are substantial, reducing the potential for flooding of buildings or infrastructure.

4.3. LID Recharge Efficiency Under Climate Variability and Change

[41] Evaluating LID performance based on the metric of recharge efficiency considering historical climate variability is an important first step toward forecasting recharge beneath LID considering future climate change. The inverse relation between maximum annual precipitation intensity (mm) for 24 h duration storms and recharge efficiency is stronger during historical La Niña years ($r^2 = 0.68$) than during El Niño years ($r^2 = 0.21$) (Figure 10b). The Mission Dolores station data indicate that storm intensity is generally less during La Niña years than El Niño years. For example, between 1954 and 2012, only three storms during La Niña years compared to seven storms during El Niño years exceeded the 17 mm hr^{-1} intensity for a 1 h event with a 5 year return period, which is often the design storm on the intensity-duration-frequency (IDF) curve that is used for urban storm water retention. El Niño and La Niña years with 1 h precipitation events that exceed the 5 year design storm have some of the lowest recharge efficiencies (Figure 10b).

[42] Evaluating recharge efficiency under future El Niño years is particularly relevant given the GFDL A1F1 forecasted 8.0% increase in winter precipitation in the 21st century that may be associated with El Niño-like precipitation. Based on the IDF curve for the Mission Dolores station data, modifying the design of the infiltration trench and increasing the storage capacity to 20 m^3 should be able to capture 100% of storm water from all 1 h, 6 h, and 24 h duration events with return periods of 2 year, 5 year, 10 year, and 25 years, except for the 24 h duration storms with 10 year and 25 year return periods. Additional work is needed to evaluate if a larger storage capacity would increase the recharge efficiency considering the GFDL A1F1 forecasted 11% increase in high intensity (>8.0 mm) 24 h duration events in the 21st century.

[43] San Francisco and many coastal cities around the world are vulnerable to rising sea levels that, combined with overpumping of groundwater to support a growing coastal population, greatly increases the risk of seawater intrusion in coastal aquifers [*Green et al*., 2011]. Adaptation approaches such as LID BMPs will become more important in water-resource management, particularly in urban, coastal aquifers that are susceptible to seawater intrusion. LID BMPs can mitigate the impacts from intense events by capturing storm water and increasing recharge and groundwater storage that increases hydraulic head in coastal aquifers and may help reduce seawater intrusion and control land subsidence in areas of groundwater pumping. Future research is needed to upscale our findings across a coastal city and test our hypothesis that the use of small scale, spatially distributed LID BMPs that enhance recharge may help to mitigate seawater intrusion in coastal aquifers. Findings from this study advance the understanding of urban recharge, particularly beneath LID BMPs, and can be used to help guide adaptive management plans under growing populations and climate variability and change.

5. Conclusions

[44] We used a variety of in situ and modeling methods to quantify and compare controlling processes on urban recharge rates and volumes beneath a LID BMP infiltration trench and irrigated lawn under current (2011–2012), historical (1954–2012), and future (2099–2100) climate variability and change. We conclude that the in situ and modeling methods are complementary, particularly for simulating historical and future recharge scenarios, and the in situ measurements of matric potential, water content, and drainage rates are critical for accurately estimating recharge under current conditions. Recharge rates were an order of magnitude greater beneath the infiltration trench than beneath the irrigated lawn. Yet the volume of recharge was estimated to be an order of magnitude greater beneath the irrigated lawn with similar area as the drainage area of the infiltration trench. This inconsistency between recharge rates and volumes beneath the infiltration trench was a function of the relatively smaller inflow volumes to the infiltration trench as compared to the irrigated lawn. Additionally, increasing the storage capacity will likely help to improve the performance of the infiltration trench in capturing and retaining storm water and increasing the current recharge efficiencies of 58–79%.

[45] **Acknowledgments.** Funding for this research was provided by the 2011 Geological Society of America Graduate Student Research Grant, the G.A. Harris Research Instrumentation Grant from Decagon Devices, Inc., San Francisco State University ORSP-FOA 2010–11, and the Research Institute for Humanity and Nature (RIHN) R-08-Init (water-energy-food nexus) project. We thank Zip Akyurek, Ryan Corbett, Mays Danfoura, Phil Evans, Ryan Ford, Gabby Geyer, Elizabeth Peters, Drew Potter, Carrie Thomas, Elzie Velasco, and Davin Wentworth-Thrasher

(San Francisco State University) for assistance with the installation, monitoring, and maintenance of the field sites.

References

Ando, A. W., and L. P. C. Freitas (2011), Consumer demand for green stormwater management technology in an urban setting: The case of Chicago rain barrels, *Water Resour. Res.*, *47*, W12501, doi:10.1029/2011WR011070.

Barbu, I. A., T. P. Ballestero, and R. M. Roseen (2008), LID-SWM practices as a means of resilience to climate change and it's effects on groundwater recharge, in *Groundwater Resources Management: Adaptation Measures to Water Scarcity Science and Policy Responses*, p. 13, Univ. of Calif., Irvine.

Bouwer, H., and R. C. Rice (1984), Hydraulic properties of stony vadose zones, *Ground Water*, *22*(6), 696–705.

California Stormwater Quality Association (2003), *Stormwater Best Management Practices: Handbook New Development and Redevelopment*, 378 p., Menlo Park, Calif. [Available at http://www.cabmphandbooks.com/documents/Development/DevelopmentHandbook.pdf, last accessed 23 Nov. 2013.].

Cantone, J., and A. Schmidt (2011), Improved understanding and prediction of the hydrologic response of highly urbanized catchments through development of the Illinois Urban Hydrologic Model, *Water Resour. Res.*, *47*, W08538, doi:10.1029/2010WR009330.

Cayan, D. R., R. Webb, H. F. Diaz, and V. Markgraf (1992), El Niño Southern Oscillation and streamflow in the western United States, in *El Niño: Historical and Paleoclimatic Aspects of the Southern Oscillation*, edited by H. F. Diaz and V. Markgraf, pp. 29–68, Cambridge Univ. Press, New York.

Cayan, D. R., E. P. Maurer, M. D. Dettinger, M. Tyree, K. Hayhoe, C. Bonfils, P. Duffy, and B. Santer (2006), Climate scenarios for California, Final White Paper From Calif. Clim. Change Cent., *Publ. CEC-500–2005-203-SF*. California Environmental Protection Agency, Sacramento, Calif. [Available at http://www.climatechange.ca.gov/climate_action_team/reports/index.html.]

Cayan, D. R., E. P. Maurer, M. D. Dettinger, M. Tyree, and K. Hayhoe (2007), Climate change scenarios for the California region, *Clim. Change*, *87*, S21–S42, doi:10.1007/s10584-007-9377-6.

Clifton, H. E., R. E. Hunter, and J. V. Gardner (1988), Analysis of eustatic, tectonic, and sedimentologic influences on transgressive and regressive cycles in the Upper Cenozoic Merced Formation, San Francisco, California, in *New Perspectives in Basin Analysis*, edited by K. L. Kleinspehn and C. Paola, pp. 109–128, Springer, New York.

Crawley, M. J. (2007), *The R Book*, John Wiley, Chichester, U. K.

Davis, A. P. (2008), Field performance of bioretention: Hydrology impacts, *J. Hydrol. Eng.*, *13*, 90.

Davis, A. P., W. F. Hunt, R. G. Traver, and M. Clar (2009), Bioretention technology: Overview of current practice and future needs, *J. Environ. Eng.*, *135*(3), 109–117, doi:10.1061/(ASCE)0733–9372(2009)135:3(109).

Dettinger, M. D., and D. R. Cayan (1994), Large-scale atmospheric forcing of recent trends toward early snowmelt runoff in California, *J. Clim.*, *8*, 606–624.

Dettinger, M. D., D. S. Battisti, R. D. Garreaud, G. J. McCabe, and C. M. Bitz (2001), Interhemispheric effects of interannual and decadal ENSO-like climate variations on the Americas, in *Interhemispheric Climate Linkages*, edited by V. Markgraf, pp. 1–16, Academic Press, San Diego, Calif.

Devinny, J. S., S. Kamieniecki, and M. Stenstrom (2005), *Alternative Approaches to Stormwater Quality Control*, 93 pp., Cent. for Sustainable Cities, Univ. of South. Calif., Los Angeles. [Available at http://www.seas.ucla.edu/stenstro/r/r49.pdf, last accessed 17 Aug. 2012.].

Dietz, M. E. (2005), Rain garden design and function: A field monitoring and computer modeling approach, dissertation, Univ. of Conn., Department of Natural Resources Management and Engineering, Storrs, Conn.

Dietz, M. E. (2007), Low impact development practices: A review of current research and recommendations for future directions, *Water Air Soil Pollut.*, *186*(1–4), 351–363, doi:10.1007/s11270-007-9484-z.

Dietz, M. E., and J. C. Clausen (2005), A field evaluation of rain garden flow and pollutant treatment, *Water Air Soil Pollut.*, *167*(1–4), 123–138, doi:10.1007/s11270-005-8266-8.

Dietz, M. E., and J. C. Clausen (2006), Saturation to improve pollutant retention in a rain garden, *Environ. Sci. Technol.*, *40*(4), 1335–1340, doi:10.1021/es051644f.

Dietz, M. E., and J. C. Clausen (2008), Stormwater runoff and export changes with development in a traditional and low impact subdivision, *J. Environ. Manage.*, *87*(4), 560–566, doi:16/j.jenvman.2007.03.026.

Earman, S., and M. D. Dettinger (2011), Potential impacts of climate change on groundwater resources—A global review, *J. Water Clim. Change*, *2*(4), 213–229.

Endreny, T., and V. Collins (2009), Implications of bioretention basin spatial arrangements on stormwater recharge and groundwater mounding, *Ecol. Eng.*, *35*(5), 670–677, doi:10.1016/j.ecoleng.2008.10.017.

Enfield, D. B., A. M. Mestas-Nunez, and P. J. Trimble (2001), The Atlantic Multidecadal Oscillation and its relationship to rainfall and river flows in the continental U.S., *Geophys. Res. Lett.*, *28*, 2077–2080.

Ermilio, J. R., and R. G. Traver (2006), Hydrologic and pollutant removal performance of a bio-infiltration BMP, in *World Environmental and Water Resource Congress 2006: Examining the Confluence of Environmental and Water Concerns*, edited by R. Graham, pp. 1–12, American Society of Civil Engineers, Reston, Va., doi: 10.1061/40856(200)394.

Fleming, S. W., and E. J. Quilty (2007), Aquifer responses to El Nino-Southern Oscillation, southwest British Columbia, *Ground Water*, *44*(4), 595–599, doi:10.1111/j.1745–6584.2006.00187.x.

Fowler, H. J., S. Blenkinsop, and C. Tebaldi (2007), Linking climate change modelling to impacts studies: Recent advances in downscaling techniques for hydrological modelling, *Int. J. Climatol.*, *27*, 1547–1578, doi:10.1002/joc.1556.

Green, T. R., M. Taniguchi, and H. Kooi (2007), Potential impacts of climate change and human activity on subsurface water resources, *Vadose Zone J.*, *6*(3), 531–532.

Green, T. R., M. Taniguchi, H. Kooi, J. J. Gurdak, D. Allen, H. Treidel, and A. Aureli (2011), Beneath the surface of global change: Impacts of climate change on groundwater, *J. Hydrol.*, *405*, 532–560, doi:10.1016/j.jhydrol2011.05.002.

Guilyardi, E., A. Wittenberg, A. Fedorov, M. Collins, C. Wang, A. Capotondi, G. J. van Oldenborgh, and T. Stockdale (2009), Understanding El Niño in ocean-atmosphere general circulation models: Progress and challenges, *Bull. Am. Meteorol. Soc.*, *90*(3), 325–340, doi:10.1175/2008BAMS2387.1.

Guo, Y., S. Liu, and B. W. Baetz (2012), Probabilistic rainfall-runoff transformation considering both infiltration and saturation excess runoff generation processes, *Water Resour. Res.*, *48*, W06513, doi:10.1029/2011WR011613.

Gurdak, J. J., R. T. Hanson, P. B. McMahon, B. W. Bruce, J. E. McCray, G. D. Thyne, and R. C. Reedy (2007), Climate variability controls on unsaturated water and chemical movement, high plains aquifer, USA, *Vadose Zone J.*, *6*(3), 533–547, doi:10.2136/vzj2006.0087.

Gurdak, J. J., R. T. Hanson, and T. R. Green (2009), Effects of climate variability on groundwater resources of the United States, *U.S. Geol. Surv. Fact Sheet, 2009–3074*, 4 pp. [Available at http://pubs.usgs.gov/fs/2009/3074/, last accessed 6 Mar. 2012.].

Hanson, R. T., M. W. Newhouse, and M. D. Dettinger (2004), A methodology to asess relations between climatic variability and variations in hydrologic time series in the southwestern United States, *J. Hydrol.*, *287*(1–4), 252–269.

Hanson, R. T., W. Schmid, C. C. Faunt, and B. Lockwood (2010), Simulation and analysis of conjunctive use with MODFLOW's farm process, *Ground Water*, *48*(5), 674–689, doi:10.1111/j.1745–6584.2010.00730.x.

Healy, R. W. (2010), *Estimating Groundwater Recharge*, 245 p., Cambridge Univ. Press, Cambridge, U. K.

Helsel, D. R., and R. M. Hirsch (2002), *Statistical Methods in Water Resources, Tech. of Water Resour. Invest. Book 4*, U.S. Geol. Surv., Reston, Va. [Available at http://pubs.usgs.gov/twri/twri4a3/.]

Holman, I. P., M. Rivas-Casado, N. J. K. Howden, J. P. Bloomfield, and A. T. Williams (2009), Linking North Atlantic ocean-atmosphere teleconnection patterns and hydrogeological responses in temperate groundwater systems, *Hydrol. Processes*, *23*, 3123–2126.

Holman, I. P., M. Rivas-Casado, J. P. Bloomfield, and J. J. Gurdak (2011), Identifying non-stationary groundwater level response to North Atlantic ocean-atmosphere teleconnection patterns using wavelet coherence, *Hydrogeol. J.*, *19*(6), 1269–1278, doi:10.1007/s10040-011-0755-9.

IPCC (2007), *Climate Change 2007: Synthesis Report. Contribution of Working Groups I, II and III to the Fourth Assessment Report of the Intergovernmental Panel on Climate Change*, Geneva, Switz.

Labat, D. (2008), Wavelet analysis of the annual discharge records of the world's largest rivers, *Adv. Water Resour.*, *31*(1), 109–117, doi:10.1016/j.advwatres.2007.07.004.

Laws, B. V., E. R. V. Dickenson, T. A. Johnson, S. A. Snyder, and J. E. Drewes (2011), Attenuation of contaminants of emerging concern during surface-spreading aquifer recharge, *Sci. Total Environ.*, *409*(6), 1087–1094, doi:10.1016/j.scitotenv.2010.11.021.

Lerner, D. (2002), Identifying and quantifying urban recharge: A review, *Hydrogeol. J.*, *10*(1), 143–152, doi:10.1007/s10040-001-0177-1.

Lerner, D. N. (1990), Groundwater recharge in urban areas, *Atmos. Environ., Part B*, *24*(1), 29–33, doi:10.1016/0957-1272(90)90006-G.

Maimone, M., D. E. O'Rourke, J. O. Knighton, and C. P. Thomas (2011), Potential impacts of extensive stormwater infiltration in Philadelphia, *Environ. Eng. Appl. Res. Pract.*, *14*(Fall), 1–12.

McCabe, G. J., M. A. Palecki, and J. L. Betancourt (2004), Pacific and Atlantic Ocean influences on multidecadal drought frequency in the United States, *Proc. Natl. Acad. Sci. U. S. A.*, *101*, 4136–4141.

McMahon, P. B., K. F. Dennehy, R. L. Michel, M. A. Sophocleous, K. Ellett, and D. B. Hurlbut (2003), Water movement through thick unsaturated zones overlying the central high plains aquifer, Southwestern Kansas, 2000–2001, *Water Resour. Invest. Rep. 03-4171*, 32 pp., U.S. Geol. Surv., Reston, Va.

McMahon, P. B., L. N. Plummer, J. K. Böhlke, S. D. Shapiro, and S. R. Hinkle (2011), A comparison of recharge rates in aquifers of the United States based on groundwater-age data, *Hydrogeol. J.*, *19*(4), 779–800, doi:10.1007/s10040-011-0722-5.

Milczarek, M., A. Graham, J. Harding, and D. Toy (2005), *Preliminary Assessment of Increased Natural Recharge Resulting From Urbanization and Stormwater Retention Within the City of Chandler*, GeoSystems Analysis, Inc., Tucson, Ariz. [Available at http://www.gsanalysis.com/Milczarek_Graham_Toy_2005.pdf, last accessed 5 Jul. 2011.]

Milczarek, M., S. Peng, L. Lacher, T. M. Yao, J. Harding, D. Goodrich, and L. Levick (2007), Prediction of groundwater recharge rates in semi-arid urbanized watersheds, paper presented at the American Water Resources Association 2007 Annual Conference, Albuquerque, N. M., GeoSystems Analysis, Inc., Tucson, Arizona, 11–15 Nov.

Miller, M. (2006), Rainwater harvesting for enhanced groundwater recharge through capture of increased runoff from site development, paper presented at the 2006 Conference on Increasing Freshwater Supplies, sponsored by Universities Council on Water Resources and National Institutes of Water Resources, OpenSIUC, Santa Fe, N. M., 18–20 Jul.

Mishra, V., and D. P. Lettenmaier (2011), Climatic trends in major U.S. urban areas, 1950–2009, *Geophys. Res. Lett.*, *38*, L16401, doi:10.1029/2011GL048255.

Moriasi, D. N., J. G. Arnold, M. W. Van Liew, R. L. Binger, R. D. Harmel, and T. L. Veith (2007), Model evaluation guidelines for systematic quantification of accuracy in watershed simulations, *Trans. Am. Soc. Agric. Biol. Eng.*, *50*(3), 885–900, doi:10.13031/2013.23153.

NOAA (2012), Climate timeseries, *GCOS Working Group on Surface Pressure*. Boulder, Colo. [Available at http://www.esrl.noaa.gov/psd/gcos_wgsp/Timeseries/, last accessed 18 Apr. 2012.]

NOAA ESRL (2012), *MEI Timeseries From Dec/Jan 1940/50 up to the Present*. Boulder, Colo. [Available at http://www.esrl.noaa.gov/psd/enso/mei/table.html, last accessed 18 Apr. 2012.]

NOAA GFDL (2012), *Geophysical Fluid Dynamics Laboratory—Welcome to GFDL*, Geophys. Fluid Dyn. Lab. Princeton, New Jersey [Available at http://www.gfdl.noaa.gov/, last accessed 13 Mar. 2012.]

NOAA NCDC (2011), *NCDC National Climatic Data Center (NCDC)*. Asheville, N. C. [Available at http://www.ncdc.noaa.gov/oa/ncdc.html, last accessed 3 Jun. 2011.]

Nzewi, O., J. A. Gilman, and G. Bartow (2010), *2009 Annual Groundwater Monitoring Report*, Westside Basin, San Francisco Publ. Utilities Comm. San Francisco, Calif. [Available at http://sfwater.org, last accessed 29 Aug. 2010.]

PC-Progress (2011), *PC-PROGRESS—Homepage*, PC-Progress Engineering Software Developer. PC-Progress, Prague, Czech Republic [Available at http://www.pc-progress.com/en/Default.aspx, last accessed 13 Jan. 2012.]

Perez-Valdivia, C., D. Sauchyn, and J. Vanstone (2012), Groundwater levels and teleconnection patterns in the Canadian Prairies, *Water Resour. Res.*, *48*, W07516, doi:10.1029/2011WR010930.

Phillips, S. P., S. N. Hamlin, and E. B. Yates (1993), Geohydrology, water quality, and estimation of ground-water recharge in San Francisco, California, 1987–1992, *WRIR 93-4019*, 69 pp., U.S. Geol. Surv., Reston, Va.

Pierce, D. W., et al. (2012), Probabilistic estimates of future changes in California temperature and precipitation using statistical and dynamical downscaling, *Clim. Dyn.*, *40*(3–4), 839–856, doi:10.1007/s00382-012-1337-9.

Pool, D. R. (2005), Variations in climate and ephemeral channel recharge in southeastern Arizona, United States, *Water Resour. Res.*, *41*, W11403, doi:10.1029/2004WR003255.

Pyke, C., M. P. Warren, T. Johnson, J. LaGro Jr., J. Scharfenberg, P. Groth, R. Freed, W. Schroeer, and E. Main (2011), Assessment of low impact development for managing stormwater with changing precipitation due to climate change, *Landscape Urban Plann.*, *103*(2), 166–173, doi:10.1016/j.landurbplan.2011.07.006.

Racz, A. J., A. T. Fisher, C. M. Schmidt, B. S. Lockwood, and M. L. Huertos (2011), Spatial and temporal infiltration dynamics during managed aquifer recharge, *Ground Water*, *50*(4), 562–570, doi:10.1111/j.1745–6584.2011.00875.x.

Richards, L. (1931), Capillary conduction of liquids in porous mediums, *Physics*, *1*, 318–333.

Ropelewski, C., and M. Halpert (1986), North American precipitation and temperature patterns associated with the El Niño/Southern Oscillation (ENSO), *Mon. Weather Rev.*, *114*, 2352–2362.

Roy-Poirier, A., P. Champagne, and Y. Filion (2010), Review of bioretention system research and design: Past, present, and future, *J. Environ. Eng.*, *136*(9), 878–889, doi:10.1061/(ASCE)EE.1943–7870.0000227.

Russo, T. A., A. T. Fisher, and D. M. Winslow (2013), Regional and local increases in storm intensity in the San Francisco Bay Area, USA, between 1890 and 2010, *J. Geophys. Res. Atmos.*, *118*, 392–3401, doi:10.1002/jgrd.50225.

Scanlon, B. R., R. W. Healy, and P. G. Cook (2002), Choosing appropriate techniques for quantifying groundwater recharge, *Hydrogeol. J.*, *10*, 18–39.

Schlea, D. A. (2011), Retention and management of stormwater runoff with rain gardens and rainwater harvesting systems, MS thesis, Grad. Prog. in Food Agric. and Biol. Eng., Ohio State Univ., Columbus, Ohio.

Schroeder, R. A. (1995), Potential for chemical transport beneath a storm-runoff recharge (retention) basin for an industrial catchment in Fresno, California, *WRIR 93–4140*, U.S. Geol. Surv., Sacramento, California.

Shang, H., J. Yan, and X. Zhang (2011), El Niño-Southern Oscillation influence on winter maximum daily precipitation in California in a spatial model, *Water Resour. Res.*, *47*, W11507, doi:10.1029/2011WR010415.

Shuster, W. D., R. Gehring, and J. Gerken (2007), Prospects for enhanced groundwater recharge via infiltration of urban storm water runoff: A case study, *J. Soil Water Conserv.*, *62*(3), 129–136.

Simunek, J., M. T. van Genuchten, and M. Sejna (2008), Development and applications of the HYDRUS and STANMOD software packages and related codes, *Vadose Zone J.*, *7*(2), 587–600, doi:10.2136/vzj2007.0077.

Stephens, D. B., M. Miller, S. J. Moore, T. Umstot, and D. J. Salvato (2012), Decentralized groundwater recharge systems using roofwater and stormwater runoff1, *J. Am. Water Resour. Assoc.*, *48*(1), 134–144, doi:10.1111/j.1752-1688.2011.00600.x.

Taylor, R., and C. Tindimugaya (2012), The impacts of climate change and rapid development on weathered crystalline rock aquifer systems in the humid tropics of sub-Saharan Africa: Evidence from south-western Uganda, in *Climate Change Effects on Groundwater Resources: A Global Synthesis of Findings and Recommendations*, edited by H. Treidel, J. L. Martin-Bordes, and J. J. Gurdak, pp. 17–32, Taylor and Francis, Boca Raton, Fla.

Taylor, R. G., et al. (2012), Ground water and climate change, *Nat. Clim. Change*, *3*(4), 322–329, doi:10.1038/nclimate1744.

Treidel, H., J. L. Martin-Bordes, and J. J. Gurdak (Eds.) (2012), *Climate Change Effects on Groundwater Resources: A Global Synthesis of Findings and Recommendations*, 401 pp., Taylor and Francis, Boca Raton, Fla.

Tremblay, L., M. Larocque, F. Anctil, and C. Rivard (2011), Teleconnections and interannual variability in Canadian groundwater levels, *J. Hydrol.*, *410*(3–4), 178–188, doi:10.1016/j.jhydrol.2011.09.013.

United Nations Educational, Scientific and Cultural Organization (2008), *Groundwater Resources Assessment Under the Pressures of Humanity and Climate Change (GRAPHIC)—A Framework Document*, Paris. [Available at http://www.unesco.org/water/ihp/graphic/media/GRAPHIC_Series_No2_WEB.pdf.]

United States Environmental Protection Agency (US EPA) (2000), Low impact development (LID), a literature review, *EPA-841-B-00–005*, 35 p., Washington, D. C.

United States Environmental Protection Agency (2009), Incorporating low impact development into municipal stormwater programs, *EPA 901-F-09-005*, 11 pp. [Available at http://www.epa.gov/region1/npdes/stormwater/assets/pdfs/IncorporatingLID.pdf.]

van Genuchten, M. T., F. J. Leij, and S. R. Yates (1991), *The RETC Code for Quantifying the Hydraulic Functions of Unsaturated Soils*, U.S. Salinity Lab., USDA, ARS, Riverside, Calif.

Vicente-Serrano, S. M., J. I. López-Moreno, L. Gimeno, R. Nieto, E. Morán-Tejeda, J. Lorenzo-Lacruz, S. Beguería, and C. Azorin-Molina (2011), A multiscalar global evaluation of the impact of ENSO on droughts, *J. Geophys. Res.*, *116*, D20109, doi:10.1029/2011JD016039.

Watershed Council: Los Angeles and San Gabriel Rivers (2000), *LA Basin Water Augmentation Study*. U.S. Environmental Protection Agency, Washington, D. C. [Available at https://wiki.epa.gov/watershed2/index.php/LA_Basin_Water_Augmentation_Study, last accessed 18 Jun 2012.]

Wolter, K., and M. S. Timlin (1993), Monitoring ENSO in COADS with a seasonally adjusted principal component index, in 17th Climate Diagnostics Workshop, pp. 52–57, National Oceanic and Atmospheric Administration (NOAA)/National Meteorological Center (NMC)/Climate Analysis Center (CAC)/National Severe Storms Laboratory (NSSL), Oklahoma Clim. Survey, CIMMS and the Sch. of Meteorol., Univ. of Okla., Norman.

Wolter, K., and M. S. Timlin (1998), Measuring the strength of ENSO events—How does 1997/1998 rank?, *Weather*, *53*(9), 315–324.

WRCC (2012), *Western Regional Climate Center*, Desert Research Institute, Reno, Nev. [Available at http://www.wrcc.dri.edu/, last accessed 24 Mar. 2012.]

Yeh, S.-W., B. P. Kirtman, J.-S. Kug, W. Park, and M. Latif (2011), Natural variability of the central Pacific El Nino event on multi-centennial time scales, *J. Geophys. Res.*, *38*, L02704, doi:10.1029/2010GL045886.